J Mol Model (2014) 20:2454
DOI 10.1007/s00894-014-2454-7

ORIGINAL PAPER

Oxygen reduction reaction on Cu-doped Ag cluster for fuel-cell cathode

Wenqiang Ma · Fuyi Chen · Nan Zhang · Xiaoqiang Wu

Received: 8 April 2014 / Accepted: 1 September 2014 / Published online: 17 September 2014

Abstract The development of fuel cells as clean-energy technologies is largely limited by the prohibitive cost of the noble-metal catalysts needed for catalyzing the oxygen reduction reaction (ORR) in fuel cells. A fundamental understanding of catalyst design principle that links material structures to the catalytic activity can accelerate the search for highly active and abundant bimetallic catalysts to replace platinum. Here, we present a first-principles study of ORR on $Ag_{12}Cu$ cluster in alkaline environment. The adsorptions of O_2, OOH, and OH on Cu-doped Ag_{13} are stronger than on Ag_{13}. The d-band centers of adsorption sites show the Cu-doping makes d-electrons transferred to higher energy state, and improves O_2 dissociation. ORR processes on $Ag_{12}Cu$ and Ag_{13} indicate Cu-doping can strongly promote ORR, and ORR process can be better preformed on $Ag_{12}Cu$ than on Ag_{13}. For four-electron transfer, the effective reversible potential is 0.401 V/RHE on $Ag_{12}Cu$ in alkaline medium.

Keyword Catalyst · Cluster · Density functional theory (DFT) · Oxygen reduction reaction (ORR) · Nanoalloy

Electronic supplementary material The online version of this article (doi:10.1007/s00894-014-2454-7) contains supplementary material, which is available to authorized users.

W. Ma (✉) · F. Chen (✉) · N. Zhang · X. Wu
State Key Laboratory of Solidification Processing, Northwestern Polytechnical University, Xi'anShaanxi, 710072, People's Republic of China
e-mail: npns_mwq@126.com
e-mail: fuyichen@nwpu.edu.cn

Introduction

The oxygen reduction reaction (ORR) on metal plays a crucial role in electrochemical energy conversion [1]. However, there are several challenging issues worth being studied in catalytic reactions of fuel cells [2–4], for example, the high price for Pt metal which is the best catalyst for H_2 and O_2 dissociation. However, the high cost of Pt has sparked a search for a Pt substitute or new ways of reducing the quantity of Pt required. For example, in contrast to Au bulk materials, Au nanoparticles can be used in many selective oxidation reactions [5–7]. Recently, the supported Pt-based alloy catalyst has received great attention because of its wide variety of advantages. Some alloyed nanoparticles, including AuPd nanoalloys [8], NaAu clusters [9], MAu (M=W, Pb, Zr, Sc, Ca) clusters [10], CuAu nanoparticles [11], and AuAg nanoalloys [12] have been disclosed in catalytic activity by first-principles calculations. Moreover, a number of highly stable mixed clusters have been produced in the laboratory, which makes it possible to design and apply the alloyed nanoparticles in catalytic chemistry [13, 14]. These indicate that different alloyed configurations could have some extra effects on catalytic processes. It would be interesting to further explore some alloyed nanoclusters of inexpensive metals for ORR. At the same time, these results emphasize the importance of understanding the catalytic property of bimetallic nanocatalysts.

The activation energy in electron transfer processes result from the interplay between solvent reorganization, orbital overlap and reaction free energy [15]. Though it is difficult to simulate process for all contained information, multiscale modeling techniques became recently available. de Morais et al. have simulated the ORR in a Pt(111)-based PEMFC [16], and Goddard III et al. have reported Multi-paradigm multi-scale simulations for fuel cell catalysts and membranes [17]. Our research is focused on intrinsic metal effects. We ignore other effects, such as support. Although such effects are

still important [18–20], we hope to gain a better understanding of the ORR on bare nanoparticles by systematically investigating how the alloyed composition affects the ORR. A clear understanding of the reaction mechanism is essential for validating the catalytic properties of new materials. The O_2 dissociation reaction is the rate determining step.

In this paper, we would like to report our recent study of O_2, OH, and OOH adsorbed on AgCu clusters using cluster model calculation. We selected Cu-doped Ag cluster as a new catalyst for ORR. ORR activity of the pure Ag or Cu is lower than Pd or Pt because O_2 adsorption energy on Ag is too low, while O_2 adsorption energy on Cu is too high [4]. Another reason is that the alloyed nanocatalyst decreases catalyst poisoning, in comparison with Pt-based catalyst [21]. Some experiments have predicted alloyed CuAg is an ORR catalyst [22–24]. We expect that each property of Ag and Cu affects O_2 adsorption on an AgCu nanoparticle and leads AgCu nanoparticle to have proper adsorption strength and to become a good catalyst for ORR. Moreover, Ag and Cu are much less expensive than Pt or Pd [25]. Although most calculations [12–16] on crystalline surface processes were done on the slab model, for our purpose, it is hard to apply this approach to discuss the pure local electronic effect of alloy cluster due to the lack of periodicity. Moreover, it allows a more direct analysis of the bonding character for local orbital, as discussed by Huang et al. [26]. Hence, the cluster model is a suitable model to be used in this study. In the direct four-electron reduction mechanism of ORR process, the O_2, OH, and OOH adsorbates are three important intermediates. It has been recognized that the origin of slow ORR kinetics is the blockage of O_2 adsorption sites by the formation of O and OH [27, 28]. Hence the study of O, OH, and OOH adsorptions are important for ORR research. The main objective of this study is to show how Cu-doping affects ORR on Cu-doped Ag clusters for fuel-cell cathode.

Methods

We simulated the ORR processes starting with the first electron transformation, following the work on a Pt(111) by Wang et al. [29–31]. These results suggest that, in an alkaline environment [32–35] a decomposition is primarily driven by the chemisorption of hydroxyl, in line with Yeager's dissociative chemisorption proposal for the first step of ORR. A unified mechanism for the first reduction step, which combines Damjanovic's [28] proton participation in the first electron reduction step and Yeager's dissociative chemisorption of O_2 is summarized as follows:

$$O_2 + * \rightarrow *-O-O \quad (1)$$

$$*-O-O + e^- + H_2O \rightarrow *-O-O-H + OH^- \quad (2)$$

or

$$O_2 + * + e^- \rightarrow *-O-O^- \quad (3)$$

$$*-O-O^- + H_2O \rightarrow *-O-O-H + OH^- \quad (4)$$

where the asterisk represents a chemisorption site on clusters. In this step, we set O_2, OOH, or OH near the adsorption site of $Ag_{12}Cu$ (or Ag_{13}) cluster at a distance of 3 Å. The optimized structures for O_2, OOH, or OH adsorption (ads) to cluster were obtained through structural optimization calculations. Then the succeeding electron transforming reactions were simulated by continuing to add H atoms (the joint efforts of one e^- from anode and one H^+ from H_2O molecule) in the system at the initiatory stage. The optimized structures for OOH, OH+OH, or OH adsorption (ads) to cluster were obtained through structural optimization calculations. For each step, we obtained the optimized structure, and calculated the adsorption energy [36] (bond strength) for those molecules on the $Ag_{12}Cu$. It is well-known that, overall, ORR can proceed by a two-step two-electron pathway with the formation of hydrogen peroxide or by a more efficient four-electron process to combine oxygen with electrons and protons directly from dissociated H_2O. Hence, the ORR on $Ag_{12}Cu$ could follow either a two-electron pathway or four-electron process, which will be examined in the simulation of subsequent electron transforming reactions. The succeeding electron transforming reactions were simulated by continuing to add H atoms in the system in the first two electron pathway. Then, we simulated the electron transforming reactions by continuing to add electrons into the modes and found the desorption of OH^- ions. The reversible potential of each reaction step on the $Ag_{12}Cu$ was also calculated following the procedure described by Roques and Anderson [37].

For an electrochemical reaction with reactants Ox and products Red:

$$O_x + e^-\left(U^0\right) \rightarrow -\mathrm{Red} \quad (5)$$

the relationship between the Gibbs free energy for a reduction reaction in aqueous (aq) solution and the reversible potential, U^0, is [37]:

$$U^0 = \Delta G^0 / nF \quad (6)$$

where ΔG^0 is the Gibbs free energy change of Eq. 5 (The free energy for a reaction is calculated as follows: $\Delta G = \Delta E + \Delta ZPE - T\Delta S$. Here the reaction energy, ΔE, and the zero point energy, ΔZPE, are obtained from DFT calculations, while the change in entropy, due to loss of translational degrees of freedom, is obtained from standard tables [38].)

For an electrochemical reaction on a catalyst surface with reactants Ox and products Red:

$$(\text{catalyst})-O_x + e^-(U) \rightarrow -(\text{catalyst})-\text{Red} \quad (7)$$

$$U = U^0 + \left(E_r - E_r^0\right)/nF \quad (8)$$

ΔE_r, is equal to the total adsorption energy of the reactants $E_{ads}(O_x)$, minus the total adsorption energy of the products E_{ads}(Red): [39, 40].

So, the reversible potential on catalyst surface U is a function of adsorption energy and standard reversible reduction potentials U^0, for the reactions in bulk solutions: [39, 40].

$$U = U^0 + \Delta E_r/nF \quad (9)$$

where U^0 is the standard solution-phase potential. Thus, if we know the reversible potential in an aqueous solution of a redox reaction U^0 (from experimental or theoretical investigations), we will be able to calculate the reversible potential on a specific catalyst surface U just by the knowledge of the adsorption energies of each species involved in the reaction. It should be noticed that the effect of charge has been considered by using the known reversible potential in an aqueous solution of a redox reaction U^0 [41] in the ORR. The predictions are very close to the experimental results [37, 39, 40].

Geometric structures of the Cu-doped and undoped Ag clusters, with adsorbed O_2, O_2^-, OOH, OOH^-, and OH, were optimized using an unrestricted density functional theory (DFT) method within the general gradient approximation in the form of RPBE (revised Perdew-Burke-Ernzerh) of functional [42]. The RPBE was specialized for oxidation and numerous other surface chemical reaction involving hydrocarbons. Semicore pseudopotential was opted together with the double numerical plus polarization (DNP) basis set for the geometric optimization [43–46]. The adsorption energies of adsorbates on the clusters were calculated according to the formula:

$$\Delta E_{\text{ads}} = E_{(\text{cluster+adsorbate})} - E_{(\text{cluster})} - E_{(\text{adsorbate})} \quad (10)$$

All computations were performed using the DMol3 software package [43, 44]. During geometrical optimization, the basis set cutoff was chosen to be 5 Å. The convergence tolerances for the geometry optimization were set to 10^{-5} Ha for the energy, 0.002 Ha/Å for the force, and 0.005 Å for the displacement. The electronic SCF tolerance was 10^{-6} Ha. A Fermi smearing of 0.005 Ha was used in all of the calculations. The DFT semicore pseudopotential proposed by Delley in 2002 [47] was employed to treat the core electrons.

Results and discussion

Adsorptions of O_2, OOH, OH

The catalytic properties of AgCu nanoparticles indicate alloyed $Ag_{12}Cu$ is a good candidate for an ORR catalyst [48]. The work shows O_2 molecule prefers to adsorb on the site with Ag and Cu atoms of AgCu cluster, too. We selected coh-Ag_{13} and Cu-doped Ag clusters as fuel-cell cathode to study ORR. The structures of Ag_{13} and $Ag_{12}Cu$ are shown in Fig. 1. The d(Ag-Ag) of Ag_{13} cluster is 2.949 Å. The d(Ag-Ag) of $Ag_{12}Cu$ cluster is in the range from 2.912 to 3.006 Å. and the d(Ag-Cu) of $Ag_{12}Cu$ cluster is about 2.728 Å. The distance between shell atom and core atom with the range from 2.729 Å to 2.986 Å in $Ag_{12}Cu$ is shorter than in Ag_{13}, which indicates Cu-doping decreases the size of cluster.

We determine the ground state of the metal clusters with the adsorbed species considered by checking their total energies with different spin multiplicity in Fig. S1 (see Supporting materials). The calculations indicate the ground state (the most stable state) of all the metal clusters with the adsorbed species is under the spin number with 0. Figure 2 and Table 1 display adsorption energies and $d_{(O-O)}$ of adsorbates on Ag_{13} and $Ag_{12}Cu$ for ORR process. The adsorption energies of O_2, O_2^-, OOH, OOH^-, 2OH, and OH on Ag_{13} are −0.216, −0.259, −1.144, −0.980, −4.594, −2.958 eV, respectively. The adsorption energies of O_2, O_2^-, OOH, OOH^-, 2OH, and OH on $Ag_{12}Cu$ are −1.019, −1.154, −1.697, −1.304, −5.405,

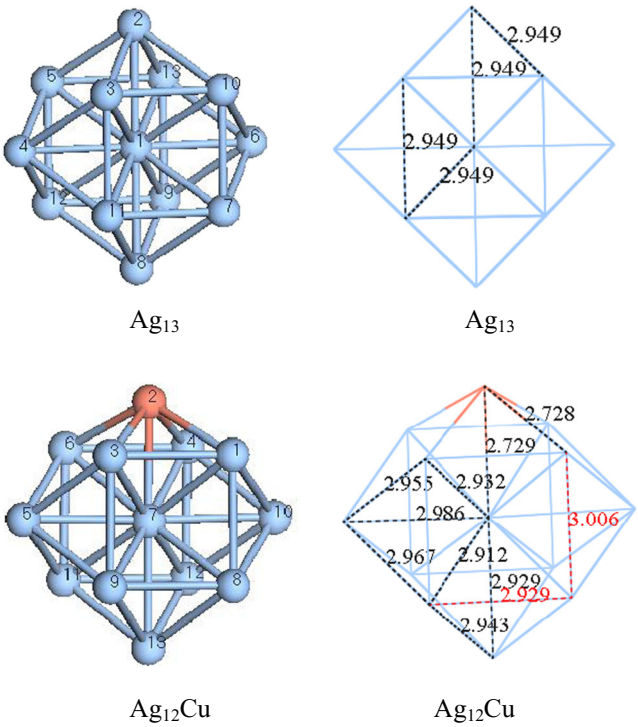

Fig. 1 the structures (*left*) and bulk lattice parameters (*right*) of optimized Ag_{13} and $Ag_{12}Cu$ clusters

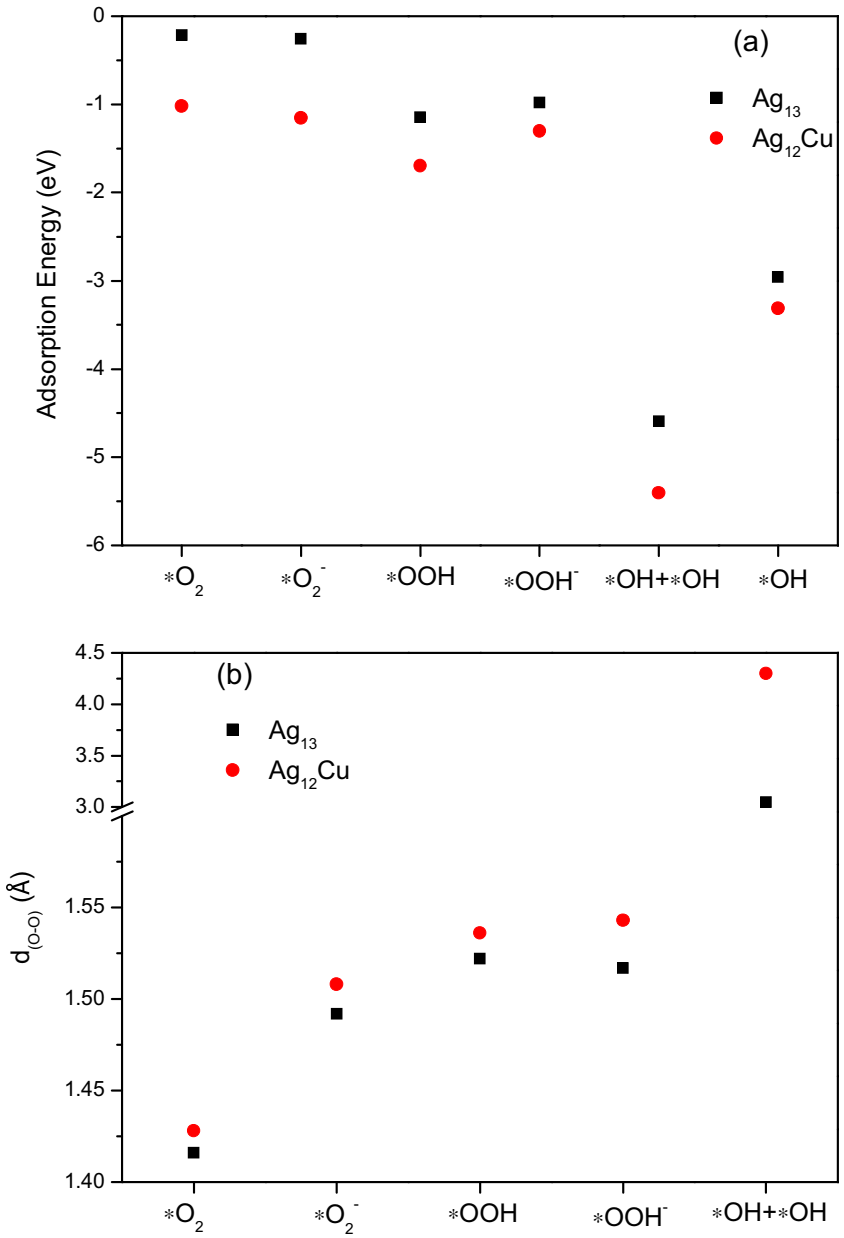

Fig. 2 Adsorption energies **a** of the adsorbates on Ag_{13} and $Ag_{12}Cu$ and the O–O bond length ($d_{(O–O)}$) for ORR process

−3.312 eV, respectively. It is obvious that the adsorption energy of O_2 (O_2^-, OOH, OOH^-, 2OH, or OH) on $Ag_{12}Cu$ is lower than that on Ag_{12} in Fig. 2a. (The adsorption energies of O_2, OOH, and OH on Ag_{13} and $Ag_{12}Cu$ compared with the ones obtained with Pt_{13} nanoclusters have been showed in Fig. S2 of Supporting materials.) So Cu-doping improves the adsorptions of adsorbates in ORR. That is to say, Cu-doping offers great conveniences for ORR. The other, $d_{(O–O)}$ (bond length) of O_2 on Ag_{13} is 1.416 Å, and $d_{(O–O)}$ of O_2 on $Ag_{12}Cu$ is 1.428 Å. The $d_{(O–O)}$ of O_2 on $Ag_{12}Cu$ is longer than that on

Table 1 Adsorption eEnergy and $d_{(O–O)}$ for O_2, OOH, OH on the Ag_{13} and$Ag_{12}Cu$

ORR pathway		$*O_2$	$*O_2^-$	*OOH	$*OOH^-$	*OH+*OH	*OH
Ag_{13}	Adsoption energy (eV)	−0.216	−0.259	−1.144	−0.980	−4.594	−2.958
	$d_{(O–O)}$ (Å)	1.416	1.492	1.522	1.517	3.047	
$Ag_{12}Cu$	Adsoption energy (eV)	−1.019	−1.154	−1.697	−1.304	−5.405	−3.312
	$d_{(O-O)}$ (Å)	1.428	1.508	1.536	1.543	4.299	

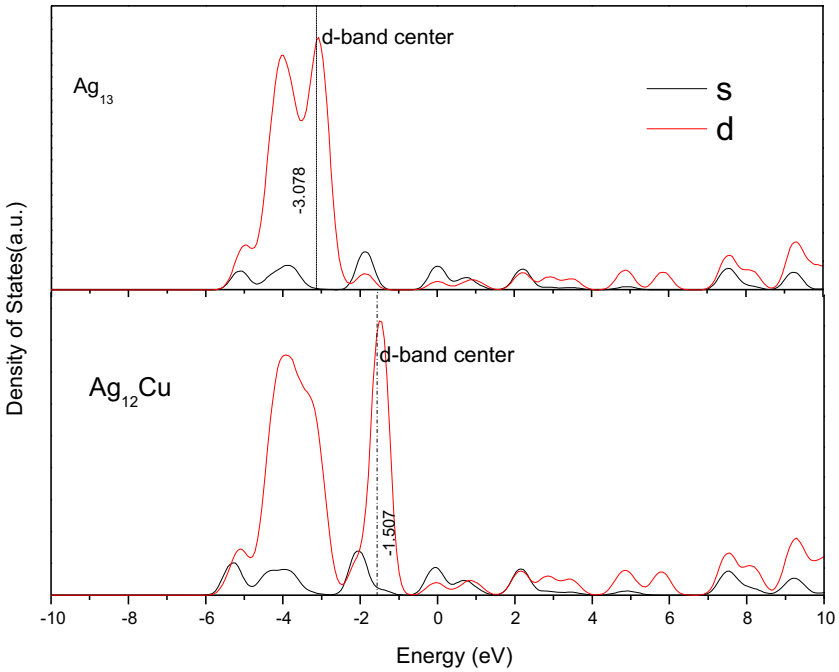

Fig. 3 Local density of states and d-band centers of three atoms located at adsorption site, and the number of these atoms is 2, 3, 10, in Ag_{13} and 1, 2, 3 in $Ag_{12}Cu$ as in Fig. 1, respectively

Ag_{12}. The $d_{(O–O)}$ of all the adsorbates on $Ag_{12}Cu$ is also longer than that on Ag_{13} as shown in Fig. 2b. Cu-doping enhances O−O dissociation in ORR process, which is propitious to ORR processes. The possible reason is that d-band center [49, 50] of adsorption site on $Ag_{12}Cu$ (−1.507 eV) is nearer Fermi level than that on Ag_{13} (−3.078 eV), as shown in Fig. 3. The d-band center on $Ag_{12}Cu$ is nearer than on Ag_{13}, which indicates Cu-doping improve energy level of d-electrons in the atoms located on adsorption site. According to d-band center theory [49, 50], the Cu-doped improves d-electrons of the atoms on adsorption site near Fermi level, and make d-electrons transferred to a relatively higher energy level, these indicates it is possible for $Ag_{12}Cu$ clusters to perform more effective catalysis. The changing of d-band center with Cu-doping is helpful for d-electrons to locate in higher energy state, and give more opportunities for s-electrons located in lower energy state. Cu-doping improve the energy level, making the silver-copper cluster perform more effective catalysis. The d-band center can be used as an indicator of the chemical activity of Ag-Cu clusters in

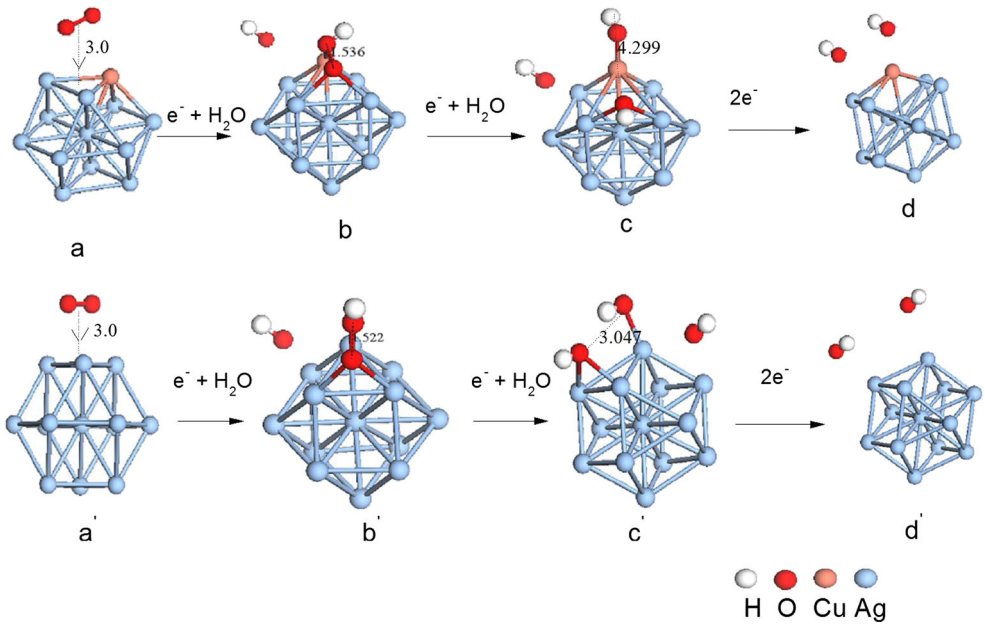

Fig. 4 Optimized structure of each electron transformation in oxygen reduction reaction: **a** adsorbs on the $Ag_{12}Cu/Ag_{13}$, **b** OOH adsorbs on the $Ag_{12}Cu$, and one OH^- group is generated, **c** O−O bond is broken, and one OH^- group is generated, **d** two OH^- are generated, and Ag−O (or Cu-O) bond is broken

Table 2 Adsorption energy difference (ΔE_r) and reversible potentials (U) of ORR step on the Ag_{13} and $Ag_{12}Cu$ (U^0 ref [29])

Reaction order	Chemical reaction	Adsorption energy difference ΔE_r(eV)		Reversible potential U^0(V/RHE)	Reversible potential U (V/RHE)	
		Ag_{13}	$Ag_{12}Cu$		Ag_{13}	$Ag_{12}Cu$
1	$O_2+H_2O+2e^-\rightarrow *OOH^-+OH^-$	0.980	1.304	−0.076	0.414	0.576
2	$*OOH^-+H_2O+2e^-\rightarrow 3OH^-$	−0.980	−1.304	0.878	0.388	0.226
Overall	$O_2+2H_2O+4e^-\rightarrow 4OH^-$	0	0	0.401	0.401	0.401

addition to that it has proved to be highly valuable in the interpretation of results on metallic surfaces. Indeed, the d-band center is not formally a chemical reactivity descriptor, the d-band center theory in principle can only be applied to periodic metal systems, and is not insensitive to the changing atom composition and size for bimetallic clusters [51, 52]. So Cu-doping improves O_2 dissociation and ORR process spontaneously.

Catalytic pathways of ORR on Ag_{13} and $Ag_{12}Cu$

We first studied catalytic pathways of Ag_{13} and $Ag_{12}Cu$. As mentioned above, there are two possible reaction pathways in the first electron transfer: (i) direct O_2 adsorption and (ii) intermediate molecule OOH adsorption. O_2 can adsorb on Ag or $Ag_{12}Cu$ in Fig. 4a. The adsorbed O_2 can further interact with an H_2O molecule and one e^- to form an adsorbed OOH. We first simulated the ORR processes beginning with the first electron transformation in an alkaline environment, in which process an intermediate molecule OOH has been formed. The simulation shows that OOH far from the Ag_{13}/$Ag_{12}Cu$ can adsorb on the Ag_{13} (or on the site with Cu+2Ag atoms of AgCu) as shown Fig. 4b (or Fig. 4b'). The dissociation energy on the adsorption site with Ag and Cu atoms is in the range from 0.65 eV to 0.9 eV, [48] while adsorption energies of OOH on $Ag_{12}Cu$ is below −1.0 eV. So an activation barrier has to be surpassed to achieve the dissociation of the O_2 molecule. It is possible for ORR process to occur spontaneously. However, the O_2 adsorption energy is −1.019 eV, over 1.5 times smaller than that for OOH adsorption (−1.6 eV) for $Ag_{12}Cu$, and the O_2 adsorption energy is −0.216 eV, over five times smaller than that for OOH adsorption (−1.0 eV) for Ag_{13}. This implies that OOH adsorption (in Fig. 4b and b') is a more favorable reaction in the first electron transfer. When adding an H_2O molecule and near the oxygen atom that attaches to the negative $Ag_{12}Cu$ or Ag_{13}, a bond is formed between the oxygen and the hydrogen atoms. At the same time, the O−O bond is broken, resulting in the formation of two hydroxide molecules (2OH), as shown in Fig. 4c or c'. During this process, the distance between the two O atoms changed from an initial value of 1.428 Å to a value of 4.99 Å on $Ag_{12}Cu$ (from an initial value of 1.416 Å to a value of 3.047 Å on Ag_{13}). The generated OH groups are bonding to the $Ag_{12}Cu$ (or Ag_{13}). This is a four-electron reaction because the O−O bond breaks during the reaction [53, 54]. After adding two more e^- to the reaction system, two OH^- are formed and completely departed from the $Ag_{12}Cu$ or Ag_{13} in Fig. 4d (or Fig. 4d'). The third and fourth electrons were then transformed in the oxygen reduction reaction. Finally, after the removal of the OH^-, the Ag_{13} (or $Ag_{12}Cu$) is ready for the next reaction cycle.

The Cu-doping also influence the reaction pathway. In addition to the reaction path listed in Table 2 (path ③ in Fig. 5), different reaction routes and catalytic behaviors were observed for Ag_{13} and $Ag_{12}Cu$. The identified reaction pathways include two-electron transfer (path ① in Fig. 5) and four electron transfer (paths ②–⑤). Path ① is a typical two-electron transfer reaction, while all other reaction paths identified are four-electron transfer reactions. The two-electron process usually is much less efficient than a four-electron one [55]. Path ② is similar to that listed in Table 2,

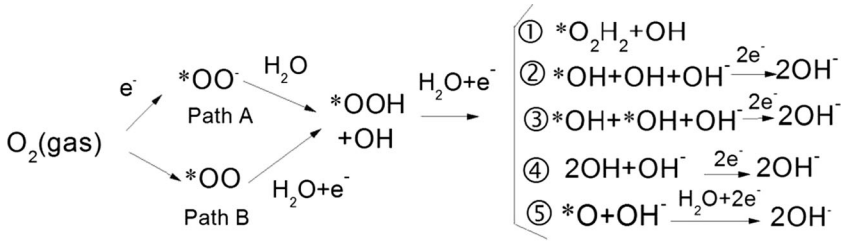

Fig. 5 Reaction scheme of ORR on Ag_{13} and $Ag_{12}Cu$ where path A presents an intermediate OOH adsorption mechanism, and path B a direct O_2 adsorption mechanism, and ①–⑤ represent five reaction pathways after OOH adsorption, ref [31]

the introduction of a hydrogen results in O−O bond breaking and formation of two OH molecules. One adsorbs on the same site as the OOH on Ag_{13} (or $Ag_{12}Cu$), while the other desorbs from adsorption site. Finally, the OH combines with e^- to form OH^-. The overall reaction reversible potential is 0.401. Path ④ is also similar to that listed in Table 2, but here, two OH molecules can be desorbed from adsorption site on $Ag_{12}Cu$ (or Ag_{13}). In the last path (path ⑤), O−O bond breaking generates an adsorbed O and one OH^- ion. H_2O further reacts with the adsorbed O with negative charge to form OH ion. The overall reversible potential is 0.401 V for Ag_{13} (or $Ag_{12}Cu$), which is equal to the standard reversible potential U^0 of oxygen and hydrogen redox reactions. This value corresponds to the standard Gibbs energy of reaction, $\Delta G^0 = 1.604$ eV, and is the maximum energy available to do electrical work.

Table 1 also displays the distance of O−O bond for *OH+*OH coadsorption. For Ag_{13}, the $d_{(O-O)}$ is 3.047 Å, and one H atom is sited between two O atoms in Fig. 4c, then H-O-H-O possibly generates. So path ① possibly takes place. On the contrary, For $Ag_{12}Cu$, $d_{(O-O)}$ with 4.229 Å is longer and makes O−O bond dissociated. Furthermore, there is not a H atom between two O atoms in Fig. 4c. So path ① is impossible for $Ag_{12}Cu$. Adsorption energy of OH on $Ag_{12}Cu$ (or Ag_{13}) in Fig. 2 shows OH group adsorbs on $Ag_{12}Cu$ (or Ag_{13}) spontaneously. So that it is impossible for $Ag_{12}Cu$ and Ag_{13} as a fuel-cell cathode to perform ORR along path ② and ④. The path ③ and ⑤ processes possibly take place on Cu-doped and undoped Ag clusters. From above analysis, we can see that Cu-doped Ag cluster is better used to make fuel-cell cathode due to efficient four-electron process.

Reversible potential of $Ag_{12}Cu$

The above chemical reactions, adsorption energy difference between reactants and products, standard reversible potential, and reversible potential on the catalyst surface are listed in Table 2. For the step of electron transformation, the reversible potential is positive, suggesting that the system moves to a more stable state during the reactions. So, the four-electron reaction can spontaneously take place on AgCu cluster. Of all the reaction steps, OOH molecular adsorption on the cluster is one of the most important steps for the catalytic reaction of oxygen reduction, because it determines whether a metal cluster electrode has catalytic activity or not. The O−O bond break is another key necessary step for the four-electron reaction. The reversible potential for overall ORR is 0.401 V (RHE) in alkaline medium, which is consistent with standard reversible potential of ORR [56, 57]. It should be noted that, during the ORR process, a 2Ag+Cu site is one active site for the ORR.

Conclusions

The DFT method was used to study the effect of Cu-doping on ORR in fuel cells. Simulation results indicates that the Cu-doping strongly affects the formation of the intermediate molecules in ORR, including OOH (or OH) adsorption, O−O bond breaking, and OH^- formation. The Cu-doping enhances the catalytic capability of the bimetallic cluster by changing the d-band center of adsorption site and reaction pathways. For four electron transfer, the predicted effective reversible potential for $Ag_{12}Cu$ is 0.401 V/RHE in alkaline medium, which is consistent with the experimental results. Engineering materials structures can promote catalytic capability of pure nanoparticles by properly doping heterogeneous elements.

Acknowledgments This study was supported by the National Natural Science Foundation of China (Grant Nos. 51271148 and 50971100), the Research Fund of State Key Laboratory of Solidification Processing in China (Grant No. 30-TP-2009), and the Aeronautic Science Foundation Program of China (Grant No. 2012ZF53073).

References

1. Stamenkovic VR, Fowler B, Mun BS, Wang GF, Ross PN, Lucas CA, Markovic NM (2007) Improved oxygen reduction activity on Pt3Ni(111) via increased surface site availability. Science 315:493–497
2. Markovic NM, Ross PN (2002) Surface science studies of model fuel cell electrocatalysts. Surf Sci Rep 45:117–229
3. Nilekar AU, Mavrikakis M (2008) Improved oxygen reduction reactivity of platinum monolayers on transition metal surfaces. Surf Sci 602:L89–L118
4. Nørskov JK, Rossmeisl J, Logadottir A, Lindqvis L, Kitchin JR, Bligaard T, Jonsson H (2004) Origin of the overpotential for oxygen reduction at a fuel-cell cathode. J Phys Chem B 108:17886–17892
5. Haruta M, Kobayashi T, Sano H, Yamada N (1987) Novel gold catalysts for the oxidation of carbon monoxide at a temperature far below 0 °C. Chem Lett 16:405–408
6. Abad A, Concepcion P, Corma A, Garcia H (2005) A collaborative effect between gold and a support induces the selective oxidation of alcohols. Angew Chem 117:4134–4137
7. Christensen CH, Jøgensen B, Rass-Hansen J, Egeblad K, Madsen R, Klitgaard SK, Hansen SM, Hansen MR, Andersen HC, Riisager A (2006) Formation of acetic acid by aqueous-phase oxidation of ethanol with Air in the presence of a heterogeneous gold catalyst. Angew Chem 118:4764–4767
8. Jirkovský JS, Panas I, Ahlberg E, Halasa M, Romani S, Schiffrin DJ (2011) Single atom hot-spots at Au—Pd nanoalloys for electrocatalytic H_2O_2 production. J Am Chem Soc 133:19432–19441
9. Molina LM, Hammer B (2005) The activity of the tetrahedral Au_{20} cluster: charging and impurity effects. J Catal 233:399–404
10. Gao Y, Shao N, Bulusu S, Zeng XC (2008) Effective CO oxidation on endohedral gold-cage nanoclusters. J Phys Chem C 112:8234–8238
11. Price SWT, Speed JD, Kannan P, Russell AE (2011) Exploring the first steps in core–shell electrocatalyst preparation: in situ characterization of the underpotential deposition of Cu on supported Au nanoparticles. J Am Chem Soc 133:19448–19458

12. Li HJ, Ho JJ (2012) Theoretical calculations on the oxidation of CO on Au55, Ag13Au42, Au13Ag42, and Ag55 clusters of nanometer size. J Phys Chem C 116:13196–13201
13. Molayem M, Grigoryan VG, Springborg M (2011) Global minimum structures and magic clusters of Cu_mAg_n nanoalloys. J Phys Chem C 115:22148–22162
14. Li WJ, Wang AQ, Liu XY, Zhang T (2012) Silica-supported Au–Cu alloy nanoparticles as an efficient catalyst for selective oxidation of alcohols. Appl Catal A 433–434:146–151
15. Quaino P, Luque NB, Nazmutdinov R, Santos E, Schmickler W (2012) Why is gold such a good catalyst for oxygen reduction in alkaline media. Angew Chem Int Ed 51:12997–13000
16. Morais RF, Sautet P, Loffred D, Franco AA (2011) A multi-scale modeling methodology to predict electrochemical observables from ab initio data: application to the ORR in a Pt(111)-based PEMFC. Electrochim Acta 56(28):10842–10856
17. Goddard W III, Merionov B, Vanduin A, Jacob T, Blanco M, Molinero V, Jang SS, Jang YH (2006) Multi-paradigm multi-scale simulations for fuel cell catalysts and membranes. Mol Simul 32(3–4):251–268
18. Bond GC, Thomson DT (1999) Catalysis by gold. Catal Rev Sci Eng 41:319–388
19. Haruta M (1997) Size- and support-dependency in the catalysis of gold. Catal Today 36:153–166
20. Hammer B (2006) Special sites at noble and late transition metal catalysts. Top Catal 37:3–16
21. Zhong WH, Liu YX, Zhang DJ (2012) Theoretical study of methanol oxidation on the PtAu(111) bimetallic surface: CO pathway *vs* non-CO pathway. J Phys Chem C 116:2994–3000
22. Kang YR, Chen FY (2013) Synthesis and application of Ag-Cu bimetallic dendrites. Acta Phys -Chim Sin 29:1712–1718
23. Kang YR, Chen FY (2013) Preparation of Ag-Cu bimetallic dendritic nanostructuresand their hydrogen peroxide electroreduction property. J Appl Electrochem 43:667–677
24. Han M, Liu SL, Zhang LY, Zhang C, Tu WW, Dai ZH, Bao JC (2012) Synthesis of octopus-tentacle-like Cu nanowire-Ag nanocrystals heterostructures and their enhanced electrocatalytic performance for oxygen reduction reaction. ACS Appl Mater Interfaces 4:6654–6660
25. Current Primary and Scrap Metal Price (2014) http://www.metalprices.com/
26. Huang YW, Chou TY, Yu GY, Lee SL (2011) Theoretical study of local electronic alloy effects of OOH, OH, and O adsorption on Pt-Pd cluster model. J Phys Chem C 115:9105–9166
27. Sepa DB, Vojnovic MV, Damjanovic A (1981) Reaction intermediates as a controlling factor in the kinetics and mechanism of oxygen reduction at platinum electrodes. Electrochim Acta 26:781–793
28. Sepa DB, Vojnovic MV, Vracar LM, Damjanovic A (1987) Different views regarding the kinetics and mechanisms of oxygen reduction at Pt and Pd electrodes. Electrochim Acta 32:129–134
29. Wang Y, Balbuena PB (2005) Ab initio molecular dynamics simulations of the oxygen reduction reaction on a Pt(111) surface in the presence of hydrated hydronium $(H_3O)^+$ $(H_2O)_2$: direct or series pathway. J Phys Chem B 109:14896
30. Yeager E (1984) Electrocatalysts for O_2 reduction. Electrochim Acta 29:1527–1537
31. Zhang LP, Niu JB, Dai LM, Xia ZH (2012) Effect of microstructure of nitrogen-doped graphene on oxygen reduction activity in fuel cells. Langmuir 28:7542–7550
32. Singh P, Buttry DA, Daniel A (2012) Comparison of oxygen reduction reaction at silver nanoparticles and polycrystalline silver electrodes in alkaline solution. J Phys Chem C 116:0656–10663
33. Hsieh CT, Pan C, Chen WY (2011) Synthesis of silver nanoparticles on carbon papers for electrochemical catalysts. J Power Sources 196: 6055–6061
34. Guo JS, Hsu A, Chu D, Chen RR (2010) Improving oxygen reduction reaction activities on carbon-supported Ag nanoparticles in alkaline solutions. J Phys Chem C 114:4323–4330
35. Varcoe JR, Slade RCT, Wright GL, Chen YL (2006) Steady-state dc and impedance investigations of H_2/O_2 alkaline membrane fuel cells with commercial Pt/C, Ag/C, and Au/C cathodes. J Phys Chem B 110:21041–21049
36. Sidik RA, Anderson AB (2006) O_2 reduction on graphite and nitrogen-doped graphite: experiment and theory. J Phys Chem B 110:1787
37. Roques J, Anderson AB (2005) Pt3Cr(111) alloy effect on the reversible potential of OOH (ads) formation from O_2 (ads) relative to Pt (111). J Fuel Cell Sci Technol 2:86–93
38. Atkins PW (1998) Physical chemistry, 6th edn. Oxford University Press, Oxford
39. Kurak KA, Anderson AB (2009) Nitrogen-treated graphite and oxygen electroreduction on pyridinic edge sites. J Phys Chem C 113: 6730–6734
40. Roques J, Anderson AB (2004) Electrode potential-dependent stages in OH_{ads} formation on the Pt_3Cr alloy (111) surface. J Electrochem Soc 151:E340–E347
41. Bard AJ, Parsons R, Jordan J (1985) Standard potentials in aqueous solution. Dekker, New York
42. Hammer B, Hansen LB, Nørskov JK (1999) Improved adsorption energetics within density-functional theory using revised perdew-burke-ernzerhof functionals. Phys Rev B 59:7413–7421
43. Delley B (1990) An All-electron numerical method for solving the local density functional for polyatomic molecules. J Chem Phys 92:508–517
44. Delley B (2000) From molecules to solids with the DMol3 approach. J Chem Phys 113:7756–7764
45. Li WY, Chen FY (2014) Structural, electronic and optical properties of 7-atom Ag-Cu nanoclusters from density functional theory. Eur Phys J D 68(91):1–11
46. Li WY, Chen FY (2014) Effect of Cu-doped site and charge on the optical and magnetic properties of 55-atom Ag cluster: a density functional theory study. 81:587–594
47. Delley B (2002) Hardness conserving semilocal pseudopotentials. Phys Rev B 66:155125–1555134
48. Shin K, Kim DH, Yeo SC, Lee HM (2012) Structural stability of AgCu bimetallic nanoparticles and their application as a catalyst: a DFT study. Catal Today 185:94–98
49. Santos E, Schmickler W (2006) d-band catalysis in electrochemistry. ChemPhysChem 7:2282–2285
50. Stamenkovic VR, Mun BS, Arenz M, Mayrhofer KJJ, Lucas CA, Wang G, Ross PN, Markovic NM (2007) Trends in electrocatalysis on extended and nanoscale Pt-bimetallic alloy surfaces. Nat Mater 6:241–247
51. Mueller T (2012) Ab initio determination of structure–property relationships in alloy nanoparticles. Phys Rev B 86:144201
52. Mokkath JH, Schwingenschlogl U (2013) Tuning the chemical activity through PtAu nanoalloying: a first principles study. J Mater Chem A 1:9885–9888
53. Walch S, Dhanda A, Aryanpour M, Pitsch H (2008) Mechanism of molecular oxygen reduction at the cathode of a PEM fuel cell: non-electrochemical reactions on catalytic Pt particles. J Phys Chem C 112:8464–8475
54. Chen RR, Li HX, Chu D, Wang GF (2009) Unraveling oxygen reduction reaction mechanisms on carbon-supported Fe-phthalocyanine and Co-phthalocyanine catalysts in alkaline solutions. J Phys Chem C 113:20689–20697
55. Gong K, Du F, Xia Z, Dustock M, Dai L (2009) Nitrogen-doped carbon nanotube arrays with high electrocatalytic activity for oxygen reduction. Science 323:760–764
56. Feng T, Anderson AB (2011) Effective reversible potential, energy loss, and overpotential on platinum fuel cell cathodes. J Phys Chem C 115:4076–4088
57. Ruvinskiy PS, Bonnefont A, Pham-Huu C, Savinova ER (2011) Using ordered carbon nanomaterials for shedding light on the mechanism of the cathodic oxygen reduction reaction. Langmuir 27:9018–9027